ORIGINAL ARTICLE

Effect of pulse width of middle-coil current on deformation behavior in electromagnetic tube forming under two-stage coils system

Xiao Zhang[1] · Shaowei Ouyang[2] · Xiaoxiang Li[2] · Liang Li[2] · Fangxiong Deng[3]

Abstract
In the majority of electromagnetic tube forming system, the distribution of Lorentz force acting on tube is restricted and has poor controllability, which leads to the tube being unable to meet the requirement of manufacturing flexibly. A new electromagnetic tube-forming method based on the two-stage coils system, which consists of two coils and two independent capacitor banks, has been proposed to improve the distribution mode and controllability of Lorentz force. With higher deformation depth and less occurrence of cracking compared with the conventional one single-coil system; this method has been proved to be effective in improving the deformation behavior of tube in electromagnetic forming through experiments. However, the deformation behavior of tube in this forming method still needs further studies. In this paper, the effect of pulse width of middle-coil current on AA1060 aluminum tube deformation behavior under two-stage coil system is investigated through simulation model, which is based on the combination of current filament method and finite element method. Results show that the short pulse width of the middle-coil current can achieve larger deformation depth of tube under relatively small discharging energy, and the long pulse width of the middle-coil current has good performance in deformed profile. Moreover, the thickness reduction in the case of long pulse width of middle-coil current is less than the case of short pulse width of the middle-coil current under equal deformation depth of tube.

Keywords Electromagnetic tube forming · Two-stage coil system · Pulse width · Tube profile · Thickness reduction

1 Introduction

The electromagnetic forming (EMF) is one kind of high-speed forming using pulsed Lorentz force acting on a metallic workpiece to deform it into the required parts [1]. Compared with conventional forming techniques, the EMF has higher forming speed, higher forming limit, and lower occurrence of spring back and wrinkling [2, 3]. Therefore, this forming technique has been widely used in sheet forming [4, 5], tube forming [6–8], joining [9], and other kinds of metal manufacturing.

In the electromagnetic tube forming, the distribution of Lorentz force is a significant factor of deformation behavior and forming performance, and the Lorentz force distribution is highly related to the structure and position of the coil. Li et al. [10] studied the tube-forming behavior by varying the relative position of coil and tube and found out the optimal range of relative position for tube flanging. Qiu et al. [11] proposed a concave coil in order to improve the forming homogeneity of the tube and acquired a homogeneous deforming range of 30% when this type of forming coil structure was adopted in electromagnetic tube expansion. However, the majority of works on electromagnetic tube forming still used conventional one single coil. As a result, occurrence of cracking on tube was relatively high with the growth of discharging energy. The main reason was that the Lorentz force mainly distributes on the middle region of tube and in radial direction, which leads to significant thickness reduction of tube wall.

✉ Fangxiong Deng
   dengfangxiong@hbust.edu.cn

1   Hubei Key Laboratory for High-efficiency Utilization of Solar
    Energy and Operation Control of Energy Storage System, Hubei
    University of Technology, Wuhan 430068, People's Republic of
    China

2   Wuhan National High Magnetic Field Center, Huazhong University
    of Science and Technology, Wuhan 430074, People's Republic of
    China

3   School of Electronic Information and Engineering, Hubei University
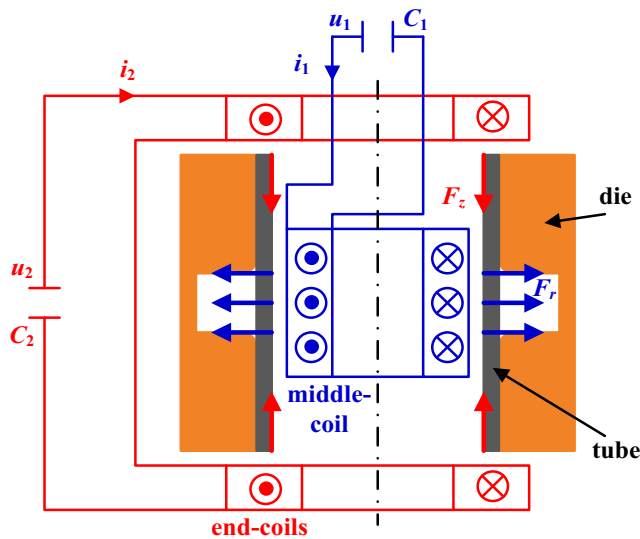   of Science and Technology, Xianning 437100, People's Republic of
    China

Fig. 1 Scheme diagram of the two-stage coil system

compression Lorentz force. Results showed that the deformation depth of tube can be increased with lower occurrence of cracking, because the thickness reduction of the tube wall is decreased. However, in both studies mentioned above, all of the forming coils were connected in series and driven by one capacitor bank. Therefore, the radial expansion Lorentz force and axial compression Lorentz force could only act on the tube synchronously, and the amplitude and acting time of both Lorentz force also could only be adjusted synchronously through altering the discharging voltage and capacitance of the capacitor bank. Thus, the controllability of the distribution of Lorentz force acting on a tube is poor and cannot meet the requirement of manufacturing flexibly. Based on the space-time–controlled multi-stage pulsed magnetic field forming and manufacturing technology proposed by Li [14], Zhang et al. [15, 16] proposed a novel electromagnetic tube-forming system, which was called "the two-stage coils system," as shown in Fig. 1. In this system, the coil placed in the central region of the tube (called "middle-coil") and the coils placed at both ends of the tube (connected in series, called "end-coils") are driven by two independent capacitor banks, to achieve the flexible control of the Lorentz force distribution on the tube. The experiment results showed that in this

To improve the distribution of Lorentz force acting on the tube, scholars introduced additional forming coils. For example, Cui et al. [12] and Qiu et al. [13] respectively proposed a method of electromagnetic tube forming in which two additional coils are placed at both ends of a tube to provide axial

Fig. 2 Equivalent circuit of the electromagnetic tube forming with one single coil
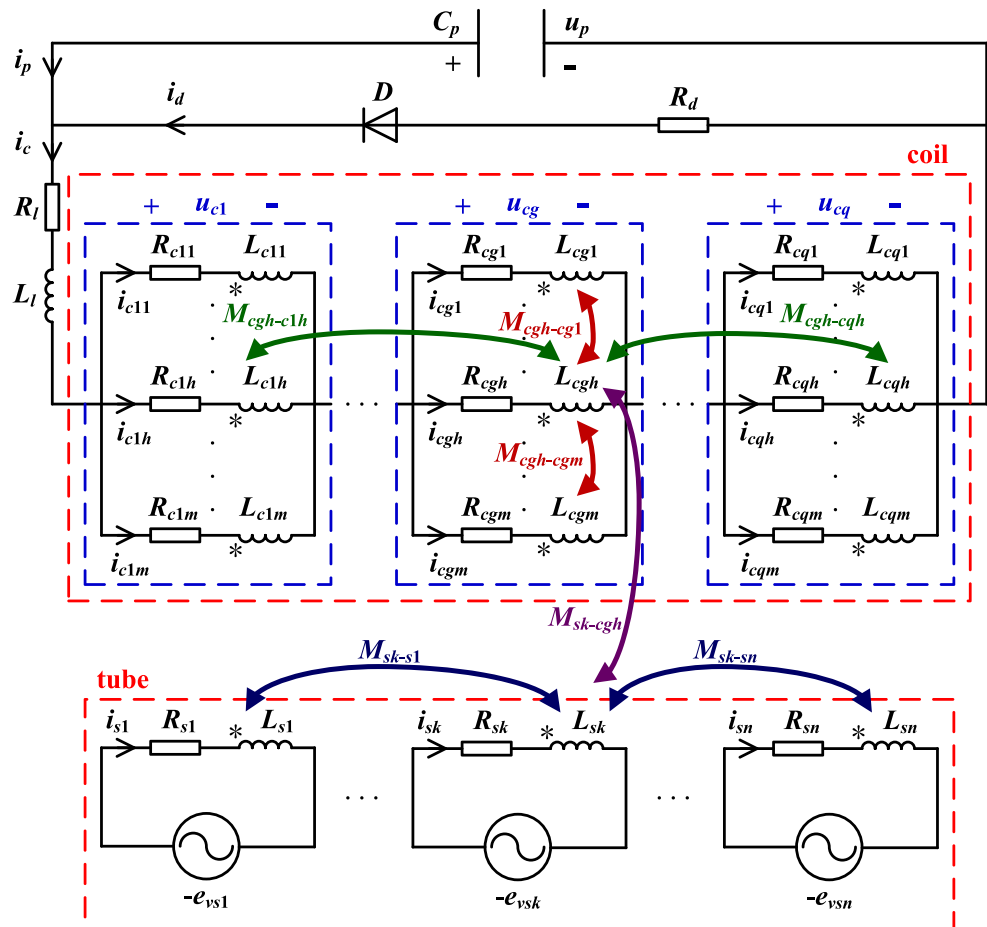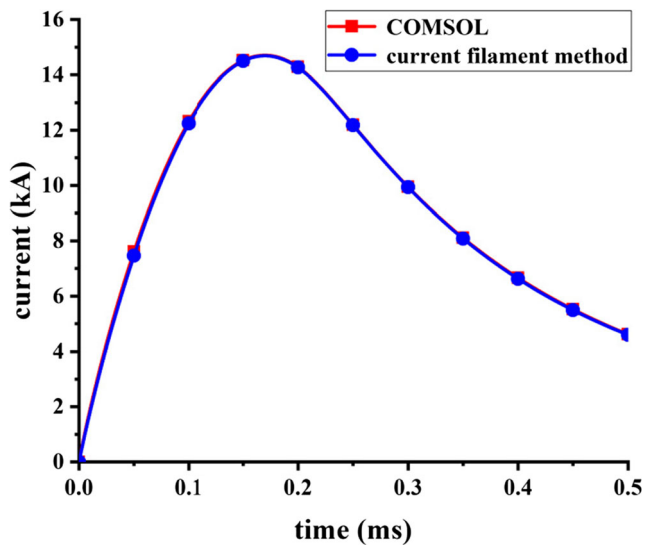
Fig. 3 Comparison of coil current waveform between the calculating result of the current filament method and the COMSOL model

forming system, the deformation depth of the tube increased, and no cracking appeared compared with conventional electromagnetic tube-forming system based on one single coil.

According to the analysis of deformation behavior of tube in electromagnetic forming with a die carried out by Zhang et al. [17], the excessive radial Lorentz force acting on the tube middle easily leads to the excessive thickness reduction of the tube wall, while the excessive axial Lorentz force acting on the tube ends leads to the overflow of the tube ends. Therefore, the optimization of radial and axial Lorentz force distribution on the tube needs to be further studied, in order to meet different requirements of manufacturing. And it can be concluded that in the proposed two-stage coils system, the optimization of the radial and axial Lorentz force distribution is
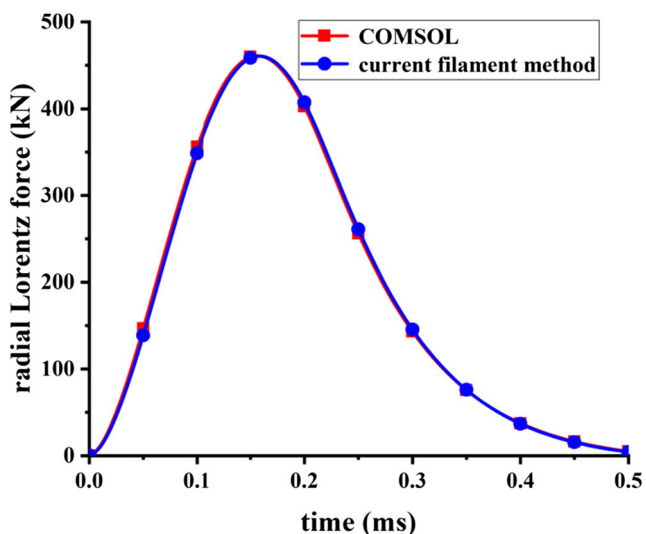

Fig. 4 Comparison of radial Lorentz force waveform between the calculating result of the current filament method and the COMSOL model

through adjusting the discharging parameters of the middle-coil and the end-coils.

In this paper, under the premise of fixed discharging parameter of the end-coils, the analysis of the effect of the middle-coil current pulse width on deformation behavior of tube in the proposed two-stage coils system was carried out through simulation. At first, the simulation model of this electromagnetic tube-forming system and the principle of the simulation model were discussed. Then, the tube deformation behaviors under different pulse width of middle-coil current were simulated and analyzed.

2 Principle of the simulation model

In the process of electromagnetic forming, the Lorentz force is generated through the interaction of the magnetic field in the space and the eddy current flows in the workpiece, and the workpiece is deformed under the action of Lorentz force. In the meantime, the deformation of the workpiece will change the geometrical parameters of the system, which leads to the changing of magnetic field distribution. The heating effect of the current also causes temperature rise in the electromagnetic forming system, but according to the research done by Cao et al. [18], the effect of temperature can be neglected, as the temperature rise of a working cycle of electromagnetic forming is relatively small. Thus, electromagnetic forming is a process of sequential coupling between the electromagnetic field model and the mechanical model [19]. However, there exists the problem that the meshes in the air region can be excessively distorted in the case of large deflection, which will lead to the convergence problem [20]. To solve this problem, the electromagnetic field model is transferred to "the current filament method," which has been applied in the analysis of induction coil gun [21], electromagnetic sheet forming [20], and electromagnetic tube forming [15].

2.1 Current filament method

The current filament method includes two steps: The first is the calculation of current flows in coil wire and eddy current flows in the tube, and the second is the calculation of Lorentz force acting on the tube.

In the first step, the coil and tube are divided into a series of equivalent circuits. In order to describe simply, the equivalent circuits of electromagnetic tube-forming model with one single coil is discussed below. In this model, the number of coil turn is q, and each turn of coil wire is divided into m count of elements. The tube is divided into n count of elements. If the divided elements are small enough, the current of each element can be treated as homogeneous distribution. Figure 2

Fig. 5 Flowchart of the simulation model
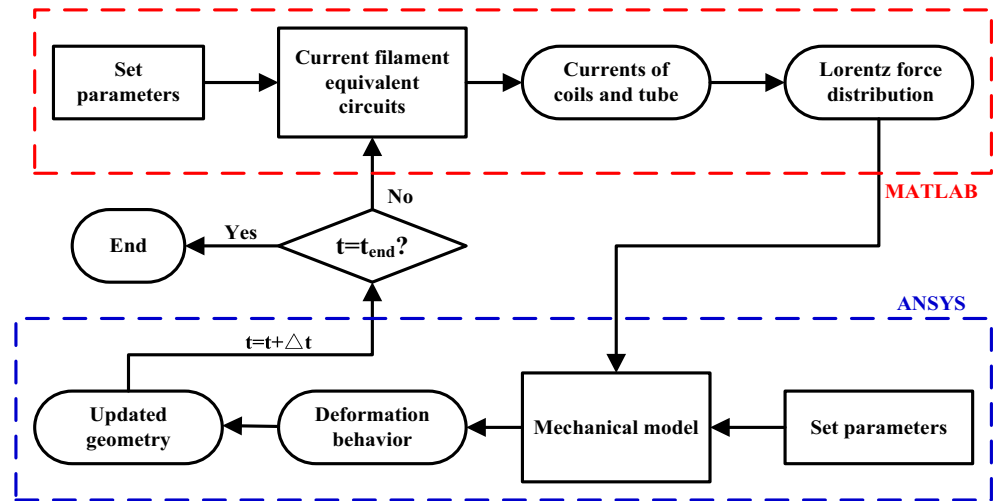
shows the equivalent circuit of electromagnetic tube forming with one single coil, from which the circuit of kth ($k = 1, ..., n$) tube element can be described as

(a)

(b)

Fig. 6 Verification of the simulation model. **a** Simulation result. **b** Experiment result

$$0 = R_{sk}i_{sk} + L_{sk}\frac{di_{sk}}{dt} + \sum_{j=1, j\neq k}^{n} M_{sk-sj}\frac{di_{sj}}{dt}$$

$$+ \sum_{g=1}^{q}\sum_{h=1}^{m} M_{sk-cgh}\frac{di_{cgh}}{dt} - e_{vskr} - e_{vskz} \quad (1)$$

where R_{sk}, L_{sk}, and i_{sk} represent the resistance, self inductance, and eddy current of the kth tube element, respectively; M_{sk-sj} represents the mutual inductance between the kth and the other tube elements, M_{sk-cgh} represents the mutual inductance between the kth tube element and the coil elements, and i_{cgh} represents the current of the hth ($h = 1, ..., m$) element of the gth ($g = 1, ..., q$) turn of coil.

The e_{vskr} and e_{vskz} in Eq. (1) represents the motional electromotive force generated by the radial and axial relative motion between the kth tube element and magnetic field, respectively, which satisfy
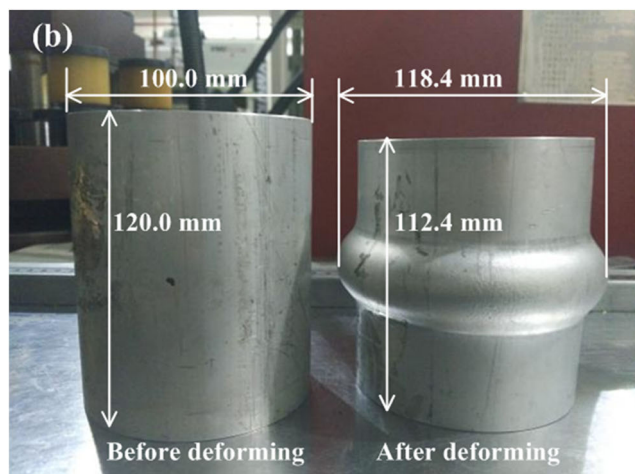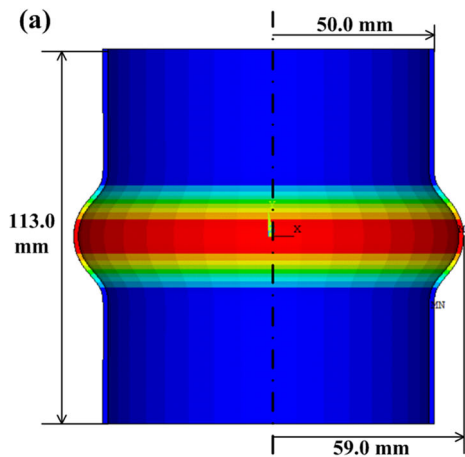
Table 1 Geometrical parameters

Symbol	Value and unit	Description
r_{c1i}	35.0 mm	Inner radius of the middle-coil
r_{c1o}	46.0 mm	Outer radius of the middle-coil
h_{c1}	40.0 mm	Length of the middle-coil
r_{c2i}	42.0 mm	Inner radius of each coil of the end-coils
r_{c2o}	53.0 mm	Outer radius of each coil of the end-coils
h_{c2}	12.0 mm	Length of each coil of the end-coils
r_{tubei}	48.0 mm	Inner radius of the tube
r_{tubeo}	50.0 mm	Outer radius of the tube
h_{tube}	200.0 mm	Length of the tube
h_{gap}	10.0 mm	Gap between the end-coils and tube ends
h_{die}	200.0 mm	Length of the die
h_g	40.0 mm	Width of the cavity of die
r_f	10.0 mm	Radius of the fillet of die

Table 2 Electromagnetic parameters

Symbol	Value and unit	Description
C_1	Variable	Capacitance of capacitor bank 1
U_1	Variable	Discharging voltage of capacitor bank 1
R_{l1}	20 mΩ	Inner resistance of power line of capacitor bank 1
L_{l1}	5 μH	Inner inductance of power line of capacitor bank 1
R_{d1}	100 mΩ	Resistance of crowbar circuit of capacitor bank 1
C_2	320 μF	Capacitance of capacitor bank 2
U_2	11.0 kV	Discharging voltage of capacitor bank 2
R_{l2}	20 mΩ	Inner resistance of power line of capacitor bank 2
L_{l2}	5 μH	Inner inductance of power line of capacitor bank 2
R_{d2}	100 mΩ	Resistance of crowbar circuit of capacitor bank 2

$$e_{vskr} = -v_{skr}\left(i_{sk}\frac{\partial L_{sk}}{\partial r} + \sum_{j=1, j\neq k}^{n} i_{sj}\frac{\partial M_{sk-sj}}{\partial r} + \sum_{g=1}^{q}\sum_{h=1}^{m} i_{cgh}\frac{\partial M_{sk-cgh}}{\partial r} \right) \quad (2)$$

$$e_{vskz} = -v_{skz}\left(i_{sk}\frac{\partial L_{sk}}{\partial z} + \sum_{j=1, j\neq k}^{n} i_{sj}\frac{\partial M_{sk-sj}}{\partial z} + \sum_{g=1}^{q}\sum_{h=1}^{m} i_{cgh}\frac{\partial M_{sk-cgh}}{\partial z} \right) \quad (3)$$

where v_{skr} and v_{skz} represent the radial and axial velocity of the kth tube element, respectively.

The circuit of the hth ($h = 1, ..., m$) element of the gth ($g = 1, ..., q$) turn of coil can be described as

$$u_{cgh} = R_{cgh}i_{cgh} + L_{cgh}\frac{di_{cgh}}{dt} + \sum_{a=1, a\neq h}^{m} M_{cgh-cga}\frac{di_{cga}}{dt}$$
$$+ \sum_{b=1, b\neq g}^{q}\sum_{h=1}^{m} M_{cgh-cbh}\frac{di_{cbh}}{dt} + \sum_{k=1}^{n} M_{cgh-sk}\frac{di_{sk}}{dt} \quad (4)$$

$$u_{cg} = u_{cg1} = \cdots = u_{cgh} = u_{cgm} \quad (5)$$

$$i_c = \sum_{h=1}^{m} i_{cgh}(g = 1, ..., q) \quad (6)$$

where u_{cgh}, R_{cgh}, and L_{cgh} represent the voltage, resistance, and self inductance of the hth element of the gth turn of coil, respectively; $M_{cgh\text{-}cga}$ represents the mutual inductance between the hth and the other elements of the gth coil turn; $M_{cgh\text{-}cbh}$ represents the mutual inductance between the hth element of the gth coil turn and all elements of the other coil turns; $M_{cgh\text{-}sk}$ represents the mutual inductance between the hth element of the gth coil turn and the tube elements; u_{cg} represents the voltage of the gth coil turn; and i_c represents the current of coil.
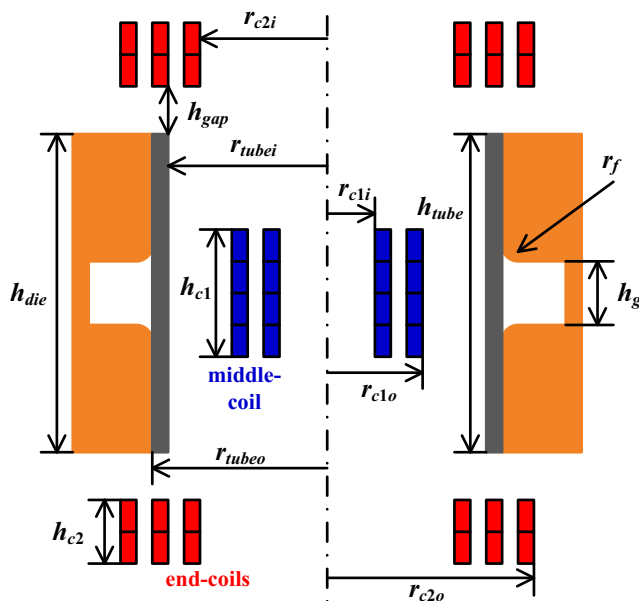

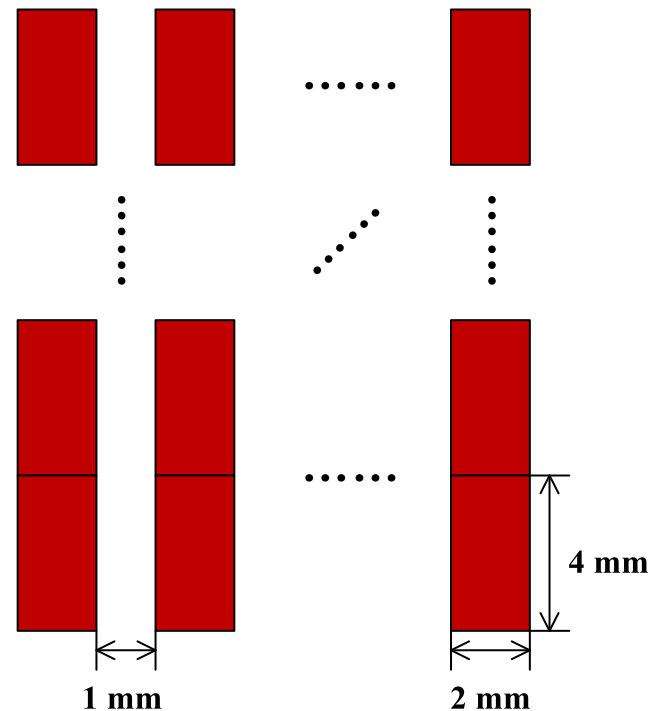**Fig. 7** Geometrical structure of the forming system

Fig. 8 Geometrical structure of the coil wires

Table 3 Three cases of equal discharging energy

Case	C_1	U_1	W_1
1	160 μF	10.0 kV	8.0 kJ
2	320 μF	7.0 kV	8.0 kJ
3	640 μF	5.0 kV	8.0 kJ

The loop of the coil and the capacitor bank satisfies

$$u_p = \left(R_l i_c + L_l \frac{di_c}{dt} \right) + \sum_{g=1}^{q} u_{cg} \tag{7}$$

$$i_p = -C_p \frac{du_p}{dt} \tag{8}$$

$$\begin{cases} i_c = i_p + i_d \\ i_d = \begin{cases} 0, & (u_p \geq 0) \\ -\dfrac{u_p}{R_d}, & (u_p < 0) \end{cases} \end{cases} \tag{9}$$

where u_p is the voltage of capacitor bank; R_l and L_l are the inner resistance and inductance of the power line, respectively; C_p is the capacitance of the capacitor bank; i_p is the current flowing out of the capacitor; and i_d and R_d are the current and resistance of the crowbar circuit [21], respectively.

From Eqs. (1) to (9), the current of all tube elements can be calculated. In other words, the eddy current distribution in the tube can be acquired.

In the second step, according to the virtual displacement method, the radial and axial Lorentz force of the kth ($k = 1, ..., n$) tube element can be described as

$$f_{skr} = i_{sk} \left(\frac{1}{2} i_{sk} \frac{\partial L_{sk}}{\partial r} + \sum_{j=1, j \neq k}^{n} i_{sj} \frac{\partial M_{sk-sj}}{\partial r} + \sum_{g=1}^{q} \sum_{h=1}^{m} i_{cgh} \frac{\partial M_{sk-cgh}}{\partial r} \right) \tag{10}$$
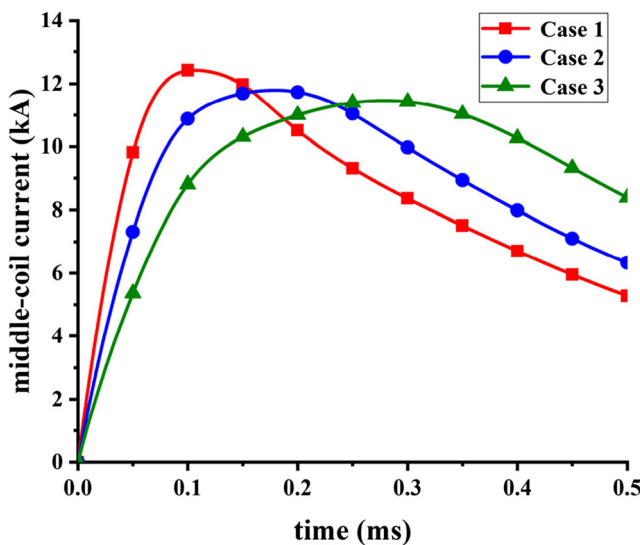
Table 4 Characteristics of the middle-coil current and radial Lorentz force under equal discharging energy W_1 of the capacitor bank 1

	Middle-coil current		Radial Lorentz force	
	Peak value	Pulse width	Intensity	Acting time
Case 1	Large	Short	Strong	Short
Case 2	Medium	Medium	Medium	Medium
Case 3	Small	Long	Weak	Long

$$f_{skz} = i_{sk} \left(\frac{1}{2} i_{sk} \frac{\partial L_{sk}}{\partial z} + \sum_{j=1, j \neq k}^{n} i_{sj} \frac{\partial M_{sk-sj}}{\partial z} + \sum_{g=1}^{q} \sum_{h=1}^{m} i_{cgh} \frac{\partial M_{sk-cgh}}{\partial z} \right) \tag{11}$$

Therefore, the Lorentz force distribution on the tube can be acquired from Eqs. (10) and (11).

A verification of the reliability of the equivalent circuits and the Lorentz force calculating method above based on current filament method has been carried out by the same electromagnetic tube-forming model built by the COMSOL Multiphysics, in which the discharging voltage is 7.0 kV, the capacitance is 320 μF, the resistance of the crowbar circuit is 100 mΩ, and the inner resistance and inductance of the power line are 20 mΩ and 5 μH, respectively. Also, in the current filament model and the COMSOL model, the coil has an inner radius of 35.0 mm, an outer radius of 46.0 mm, a length of 40.0 mm, and 40 turns of wire (the dimension is 2.0 mm × 4.0 mm per turn), and the tube has an inner radius of 48.0 mm, a length of 200.0 mm, and a thickness of 2.0 mm. The waveform of coil current and radial Lorentz force acting on the whole tube calculated in the current filament method agrees well with the corresponding waveform acquired from the COMSOL, as shown in Figs. 3 and 4. Thus, the calculating results of the current filament method have good accuracy.
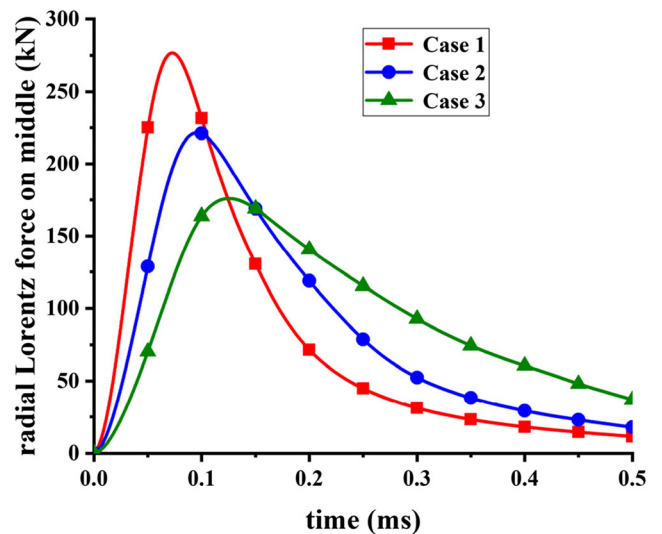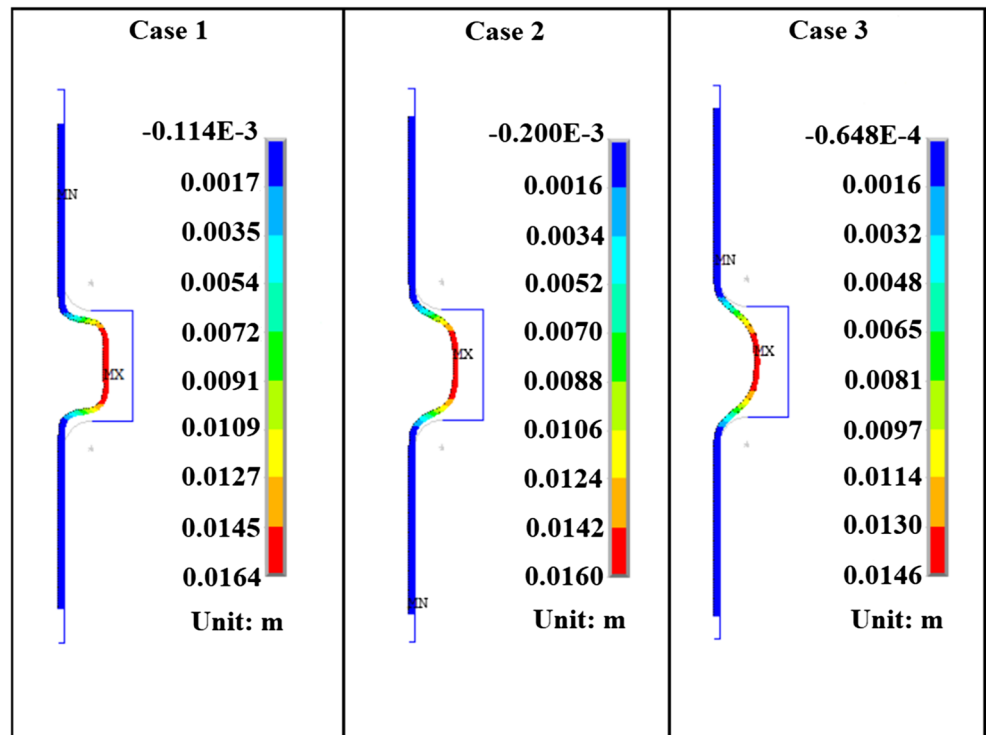

Fig. 9 Middle-coil currents under equal W_1

Fig. 10 Radial Lorentz force of middle part of tube under equal W_1

Fig. 11 Radial displacement of the deformed tubes under equal W_1

To the two-stage coils system in this work, the mutual inductance between the elements of the middle-coil and the end-coils should be taken into account on the basis of Eqs. (1) to (9).

2.2 The mechanical model

In the electromagnetic forming process, the tube is under the acting of Lorentz force, and the friction force generated from

Fig. 12 Maximum radial displacement and end flowing of tube under equal W_1

the contact between the tube and the die. Thus, the motion equation of the tube can be described as

$$f + \nabla \cdot \sigma = \rho \frac{\partial^2 d}{\partial t^2} \qquad (12)$$

where f is the total external force acting on the tube, including Lorentz force and friction force; σ is the stress tensor; ρ is the density of the tube material; and d is the displacement vector.

As the electromagnetic forming is high-speed forming, the strain rate has great influence in the forming process of the workpiece. Thus, the Cowper-Symonds model is adopted, which can be described as [22]

$$\sigma = \sigma_y \left[1 + \left(\frac{\varepsilon_p}{C} \right)^m \right] \qquad (13)$$

where σ_y is the yield stress, and ε_p is the plastic strain rate. For aluminum alloy, the parameter C equals to 6500, and m equals to 0.25.

In this work, the distribution of eddy current and Lorentz force on tube is calculated in MATLAB, and the deformation behavior of tube is simulated in ANSYS. The flowchart of the simulation model is shown in Fig. 5.

2.3 Verification of the simulation model

To verify the feasibility of the simulation model above, a comparison of the deformation result between simulation and experiment has been carried out. The experiment result
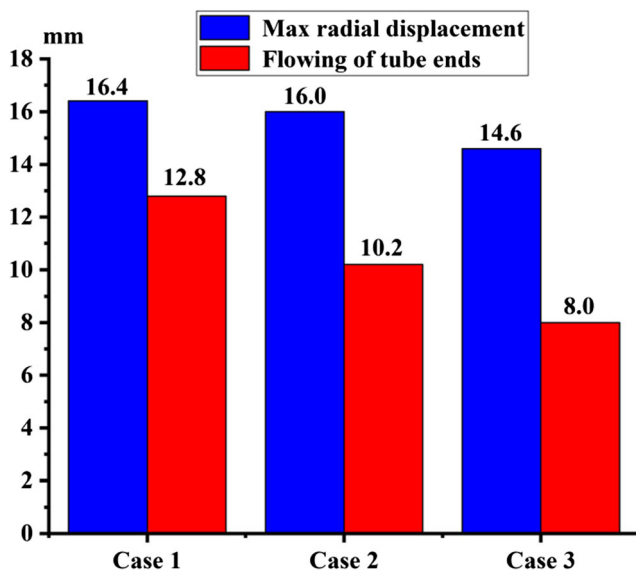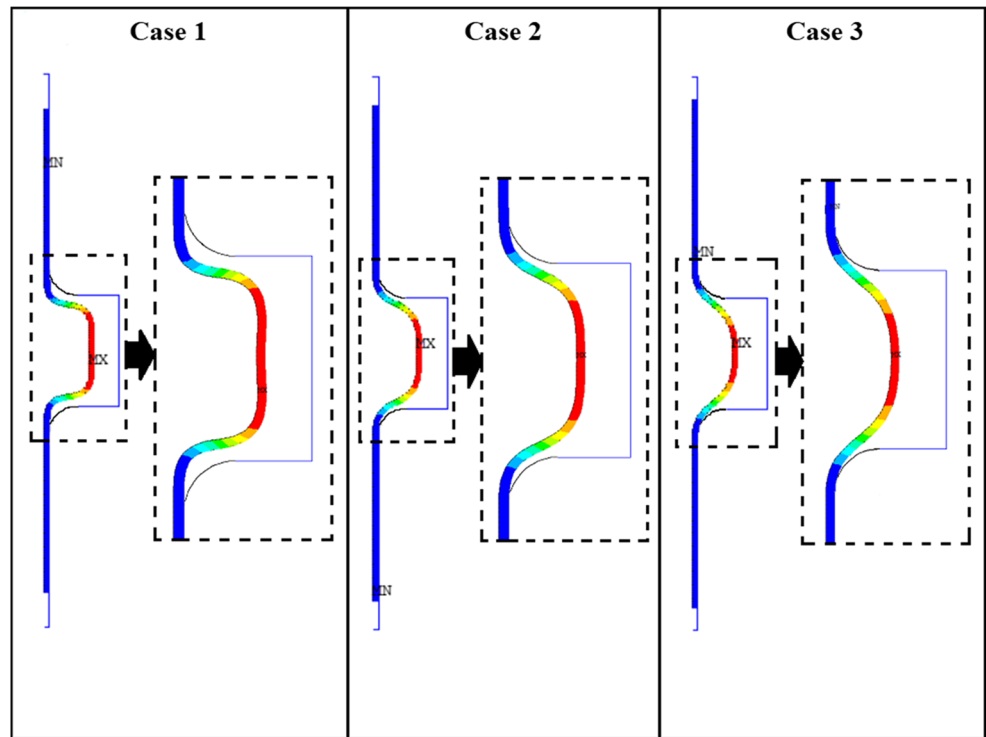
Fig. 13 Profile in the die region of the deformed tubes under equal W_1

is from our previous work, in which the aluminum tube has a length of 120.0 mm, a diameter of 100.0 mm, and a thickness of 1.5 mm. The capacitor bank related to middle-coil has a capacitance of 320 μF, and the discharging voltage is 7.0 kV. The capacitor bank related to end-coils has a capacitance of 320 μF, and the discharging voltage is 12.0 kV. The deformation result of the simulation and experiment is shown in Fig. 6, from which we can find that the deformation depth is 9.0 mm, and the end flowing is 3.5 mm in the simulation result, and the deformation depth is 9.2 mm, and the end flowing is 3.8 mm in the experiment result. The simulation result agrees well

with the experiment results, which indicates that the calculating result of the simulation model above has good reliability.

3 Results and discussions

3.1 Parameters of the forming system

In this work, the two-stage coils system consist of middle-coil, end-coils, and two capacitor banks. The middle-coil which attached to capacitor bank 1 is inside the tube and placed in
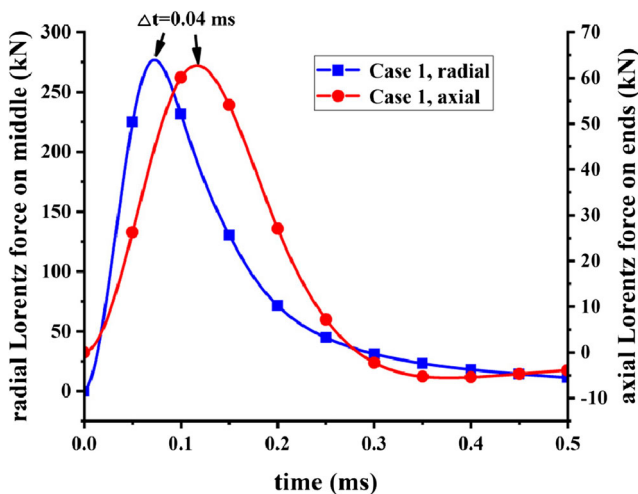

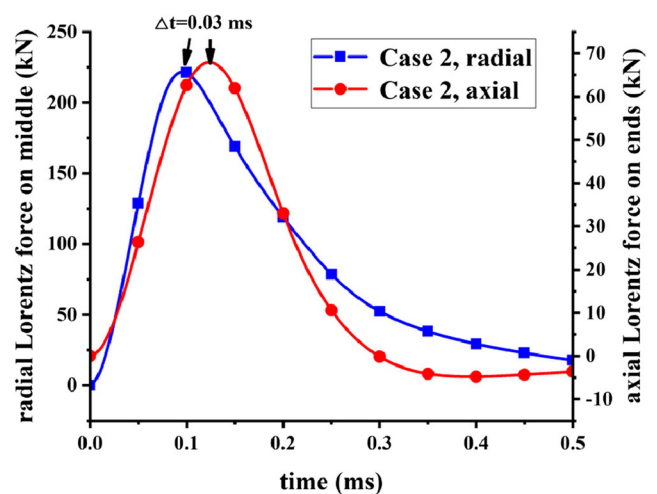**Fig. 14** Radial Lorentz force on the middle and axial Lorentz force on ends of tube in $C_1 = 160$ μF, $U_1 = 10.0$ kV

Fig. 15 Radial Lorentz force on the middle and axial Lorentz force on ends of tube in $C_1 = 320$ μF, $U_1 = 7.0$ kV

the middle region. The end-coils which attached to capacitor bank 2 consist of two coils connected in series and placed at both ends of the tube. The geometrical structure of the forming system is shown in Fig. 7. The coils are made of copper wires which has a cross-section of 2 mm (radial) × 4 mm (axial), and 1-mm space between each two layers in the radial direction, as shown in Fig. 8. The middle-coil has 4 layers in the radial direction, and each layer has 10 number of turns. Each coil of the end-coils has 4 layers in the radial direction, and each layer has 3 number of turns. The material of the tube in this study is aluminum AA1060, which has a conductivity of 3.597×10^7 S/m, a relative permeability of 1, a Young's modulus of 69 GPa, a Poisson ratio of 0.33, and an initial yield stress of 106 MPa. The geometrical parameters are shown in Table 1. The electromagnetic parameters are shown in Table 2, in which the "variable" represents the items which will be varied and discussed in the following sections. All the simulation analyses in the following sections are under the premise of equal discharging parameters of end-coils. In other words, the C_2 and U_2 are kept at 320 μF and 11.0 kV, respectively.

3.2 Simulation under equal discharging energy of capacitor bank 1

In order to initially investigate the effect of pulse width of middle-coil current, three cases are set under equal discharging energy of capacitor bank 1, as shown in Table 3. The discharging energy of capacitor bank 1 satisfies

$$W_1 = \frac{1}{2} C_1 U_1^2 \tag{14}$$

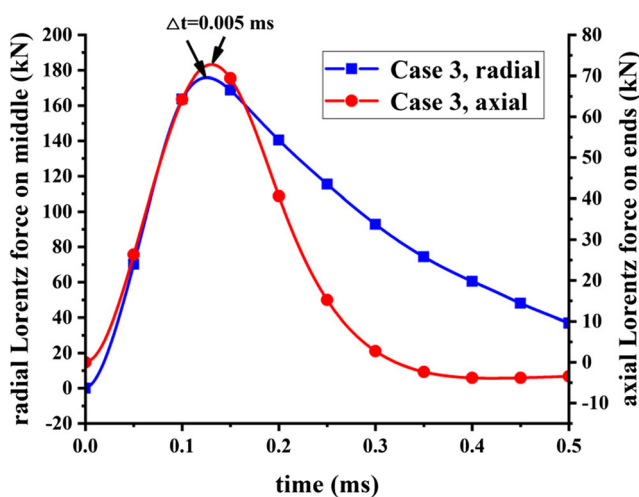where W_1 is the discharging energy, C_1 is the capacitance of capacitor bank, and U_1 is the discharging voltage.

Figure 9 shows the waveform of the middle-coil current in the three cases in which the discharging energy is equal. The waveforms show that in Case 1, the peak value of the middle-coil current is larger, but the peak time is earlier than Case 2 and Case 3, and Case 3 has the smallest peak value of the middle-coil current and the latest peak time in all the three cases. It can be concluded that when the capacitance C_1 is larger, the pulse width of the middle-coil current is longer. However, the peak value of the middle-coil current is relatively small under equal W_1 when adopting larger capacitance C_1.

To acquire the radial Lorentz force acting on tube middle, we take the middle part of the tube into account, which has a length equal to the deforming region $(h_g + 2 \times r_f)$. The waveform of the radial Lorentz force acting on the middle in the three cases are shown in Fig. 10. Compared with the corresponding cases in Fig. 9, it can be concluded that the larger the peak value of the middle-coil current, the stronger the intensity of the radial Lorentz force, and the larger the pulse width of the middle-coil current, the larger the pulse width of the radial Lorentz force. Larger pulse width indicates longer acting time of radial Lorentz force. Under equal discharging energy, the radial Lorentz force in Case 1 has the strongest intensity but the shortest acting time, while the radial Lorentz force in Case 3 has the weakest intensity but the longest acting time. The comparison of the middle-coil current and radial Lorentz force acting on the tube middle in the three cases are shown in Table 4.

Figure 11 shows the radial displacement of the deformed tubes of the three cases in which the discharging energy is equal. The maximum radial displacement of the deformed tube of Case 1, Case 2, and Case 3 is 16.4 mm, 16.0 mm, and 14.6 mm, respectively. The comparison of the maximum radial displacement and end flowing of the tube in each case is shown in Fig. 12. It can be found that Case 1 has the largest
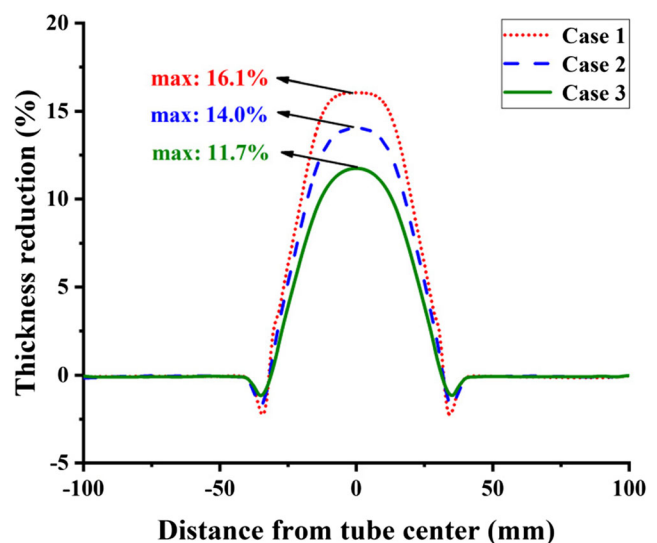

Fig. 16 Radial Lorentz force on the middle and axial Lorentz force on ends of tube in $C_1 = 640$ μF, $U_1 = 5.0$ kV

Fig. 17 Thickness reduction distribution under equal W_1

radial displacement and end flowing, which indicates that the smaller C_1, the larger radial displacement and end flowing under equal discharging energy W_1.

Figure 13 shows the deformed tube profile in the die region in the three cases. We can find that the profile of the deformed tube in Case 3 is better than that in Case 1 and Case 2, as the tube has the trend of fitting the die fillet. However, in Case 1, the tube profile cannot reach the fillet of the die, though it has larger radial deformation depth and axial end flowing than Case 3.

Figures 14, 15 and 16 show the comparison between the radial Lorentz force on the middle and axial Lorentz force on the ends of the tube in the three cases, respectively. We can find that besides the obvious difference between the radial Lorentz force acting on the tube middle, the peak value, peak time, and acting time of axial Lorentz force on the tube ends in the three cases are similar. Combining the results shown from Figs. 11, 12, 13, 14, 15 to Fig. 16, it can be concluded that the radial displacement and end flowing of the tube are determined by the radial Lorentz force acting on the tube middle and the axial Lorentz force acting on the tube ends, and the profile of the deformed tube is influenced not only by the intensity, but also by the waveform of the radial and axial Lorentz force. The detailed analyses are as follows:

1. Case 1 has the largest radial displacement and end flowing, as its radial Lorentz force acting on tube middle is obviously larger than that of Case 2 and Case 3. However, the pulse width of the radial Lorentz force is relatively short, and the peak time comes obviously earlier than the peak time of the axial Lorentz force, with
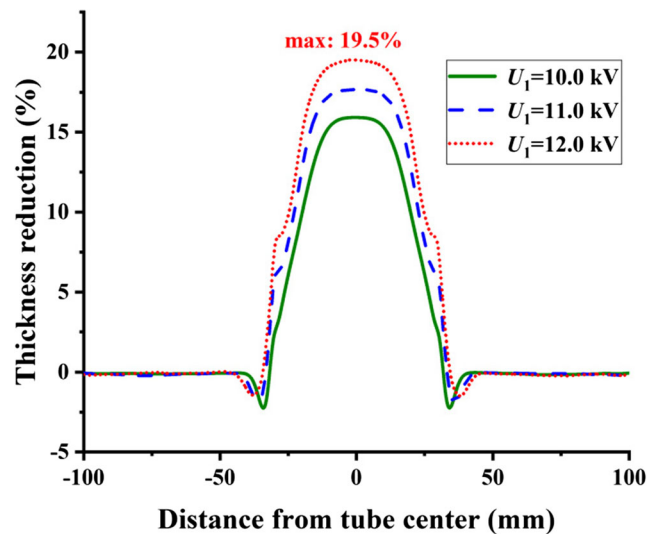

Fig. 19 Thickness reduction distribution when $C_1 = 160$ μF

time difference $\Delta t = 0.04$ ms. In this condition, the main process of the radial expansion of the tube middle is before the process of the axial flowing of the tube ends. As a result, the intensity of the radial Lorentz force on the middle is relatively weak during the process of end flowing, which leads to the overflowing of tube ends, and the deformed profile cannot reach the fillet of the die.

2. Case 2 has the medium radial displacement and end flowing in the three cases, because of the medium intensity and acting time of the radial Lorentz force. The peak time comes obviously earlier than the peak time of the axial Lorentz force, with time difference $\Delta t = 0.03$ ms, which leads to the similar characteristic of tube profile compared with Case 1.

Fig. 18 Radial displacement and deformed tube profile of $U_1 = 10.0$ kV and $U_1 = 12.0$ kV when $C_1 = 160$ μF

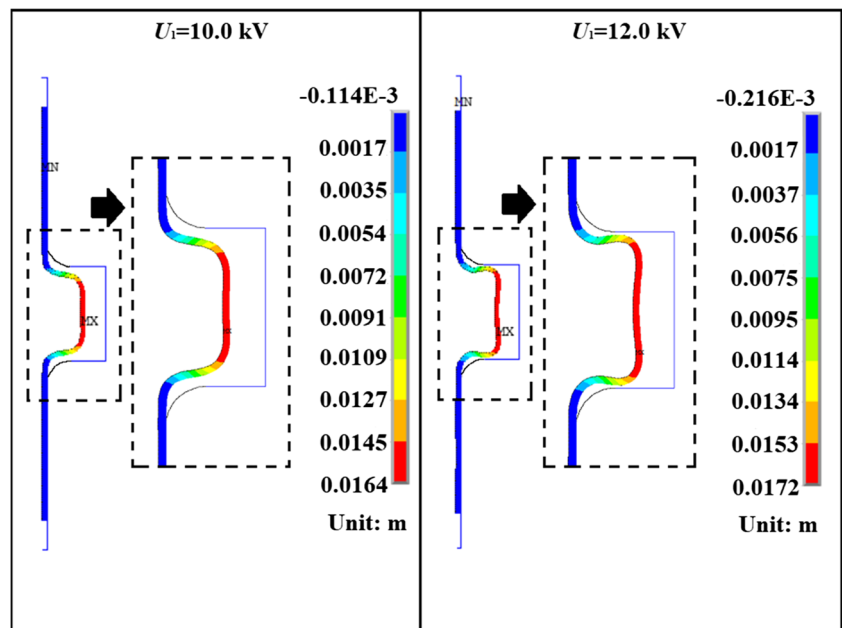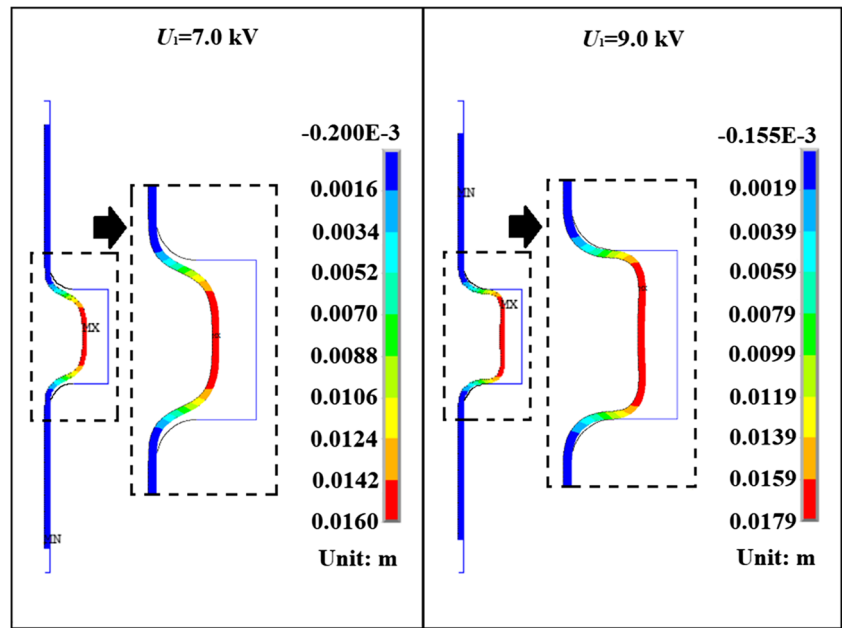**Fig. 20** Radial displacement and deformed tube profile of $U_1 = 7.0$ kV and $U_1 = 9.0$ kV when $C_1 = 320$ μF

3. In Case 3, the radial displacement and end flowing are relatively small. However, the pulse width of radial Lorentz force is longer than that of Case 1 and Case 2, and the time difference between the peak time of the radial Lorentz force and the axial Lorentz force is $\Delta t = 0.005$ ms, which is the smallest in all the three cases. In this condition, the acting time of the radial Lorentz force on the middle is relatively long, and the process of radial expansion of tube middle and the axial flowing of the tube ends are almost synchronous, which results in the best profile of deformed tube in the three cases.
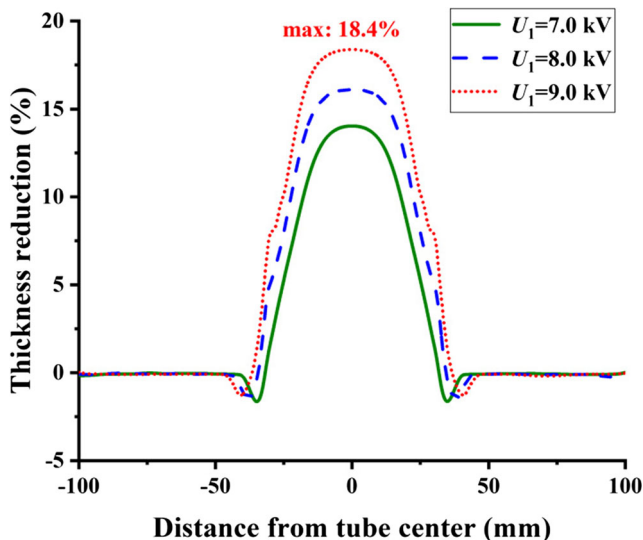

Fig. 21 Thickness reduction distribution when $C_1 = 320$ μF

Figure 17 shows the distribution of thickness reduction along the length direction of the tube in the three cases. The maximum thickness reduction of the deformed tube in Case 1, Case 2, and Case 3 are 16.1%, 14.0%, and 11.7%, respectively. It can be concluded that the deformed tube in Case 1 has the highest occurrence of cracking, because the occurrence of cracking is related to maximum thickness reduction.

3.3 Simulation under equal pulse width of middle-coil current

From Section 3.2, we can find that the larger capacitance C_1, the larger the pulse width of the middle-coil current. In this section, the effect of the pulse width of the middle-coil current is further investigated with equal C_1.

Figure 18 shows the radial displacement and the profile of the tube of $U_1 = 10.0$ kV and $U_1 = 12.0$ kV when $C_1 = 160$ μF. It can be found that when U_1 grows from 10.0 to 12.0 kV, the maximum radial displacement of the tube increases from 16.4 to 17.2 mm, while the profile of the deformed tube still cannot reach the fillet of the die. Figure 19 shows the distribution of thickness reduction along the length direction of the tube when $C_1 = 160$ μF, which shows that the thickness reduction increases as the growing of U_1, and the maximum thickness reduction reaches 19.5% when $U_1 = 12.0$ kV.

Figure 20 shows the radial displacement and profile of the tube of $U_1 = 7.0$ kV and $U_1 = 9.0$ kV when $C_1 = 320$ μF. With the growing of U_1, the maximum radial displacement of the tube increases from 16.0 to 17.9 mm, and the tube profile is obviously closer to the die profile compared with the case of $C_1 = 160$ μF, $U_1 = 12.0$ kV. Figure 21 shows the distribution of thickness reduction along the length direction of the tube

Fig. 22 Radial displacement and deformed tube profile of $U_1 = 5.0$ kV and $U_1 = 7.0$ kV when $C_1 = 640$ μF
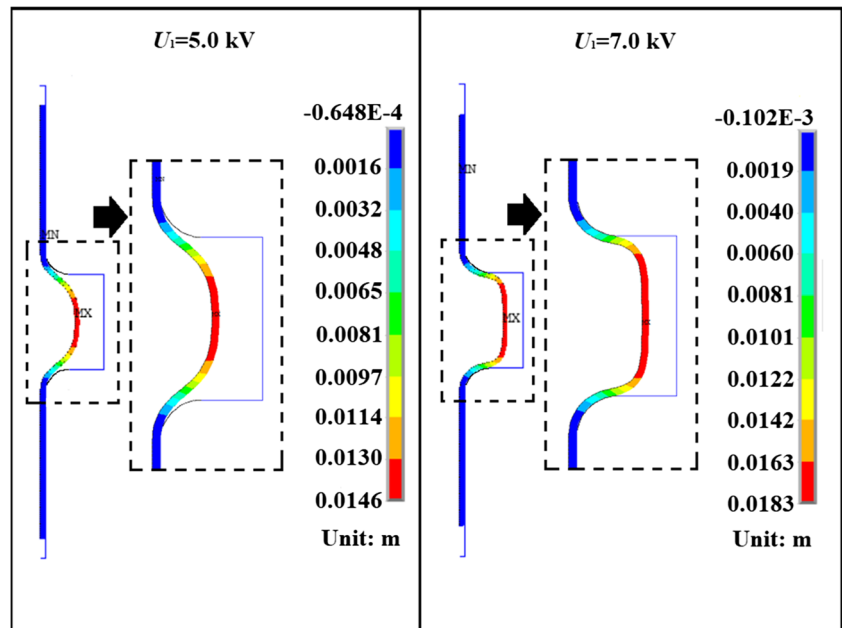
when $C_1 = 320$ μF, in which we can find that the maximum thickness reduction reaches 18.4% when $U_1 = 9.0$ kV. Compared with the case of $C_1 = 160$ μF, $U_1 = 12.0$ kV, the maximum radial displacement is 0.7 mm larger, and maximum thickness reduction is 1.1% less.

Figure 22 shows the radial displacement and profile of tube of $U_1 = 5.0$ kV and $U_1 = 7.0$ kV when $C_1 = 640$ μF. The results show that the maximum radial displacement of the tube increases from 14.6 to 18.3 mm with the U_1 growing from 5.0 to 7.0 kV. The deformed tube profile of $U_1 = 7.0$ kV fits well with the die fillet. Figure 23 shows the distribution of thickness reduction along the length direction of the tube when $C_1 = 640$ μF, which shows the maximum thickness reduction reaches 17.4% when $U_1 = 7.0$ kV. Compared with the case of

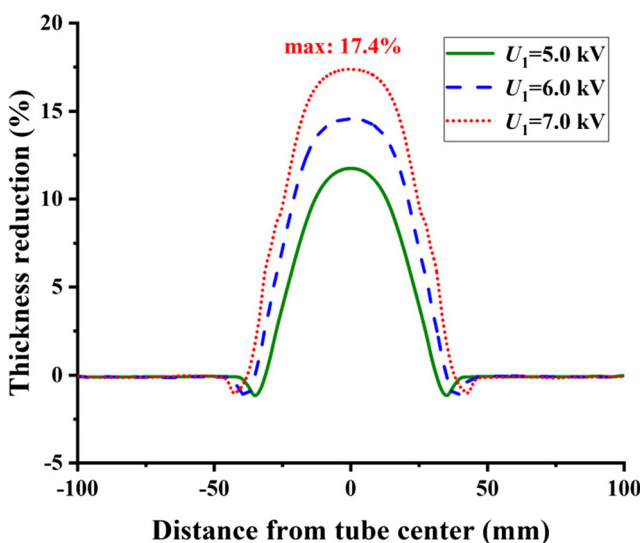$C_1 = 320$ μF, $U_1 = 9.0$ kV, the maximum radial displacement is 0.4 mm larger, and maximum thickness reduction is 1.0% less.

The comparison of the maximum radial displacement and maximum thickness reduction of the deformed tube between $C_1 = 160$ μF, $C_1 = 320$ μF, and $C_1 = 640$ μF is shown in Fig. 24. The comparison shows that when C_1 is larger, the tube can achieve larger deformation depth with less thickness reduction compared with smaller C_1. It can be predicted that under equal deformation depth, the occurrence of cracking when adopting longer pulse width of the middle-coil current
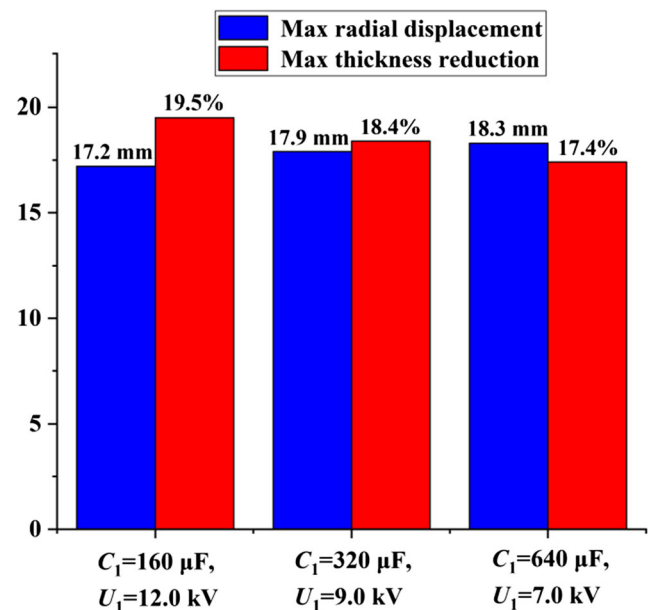

Fig. 23 Thickness reduction distribution when $C_1 = 640$ μF

Fig. 24 Comparison of maximum radial displacement and maximum thickness reduction between $C_1 = 160$ μF, $C_1 = 320$ μF, and $C_1 = 640$ μF

is less than the case using the shorter pulse width of the middle-coil current.

4 Discussion

According to the simulation investigation of the pulse width of the middle-coil current in electromagnetic tube forming with two-stage coils system under the premise of equal discharging parameters of the end-coils, which have been shown in Sections 3.2 and 3.3, we can find that:

1. To the short pulse width of middle-coil current, the intensity of radial Lorentz force acting on tube middle is stronger than that of the long pulse width of the middle-coil current under equal discharging energy of capacitor bank 1. This is beneficial for the radial displacement of the deforming region and axial flowing of tube ends. However, the occurrence of cracking is higher, as shown in Figs. 17 and 19, and the profile of the deformed tube is difficult to reach the die profile, as shown in Fig. 18. The reason is that according to Fig. 14, the acting time of radial Lorentz force is relatively short, and the peak time comes obviously earlier than the peak time of the axial Lorentz force, which leads to the asynchronous process of the radial expansion and end flowing. As a result, the tube profile is bad due to the overflowing of tube ends and the excessive increase of thickness reduction due to the excessive expansion of radial direction.

2. To the long pulse width of the middle-coil current, according to Fig. 16, the acting time of the radial Lorentz force is relatively long, and the time difference between peak time of radial Lorentz force and axial Lorentz force is relatively small. Under this condition, the process of radial expansion of tube middle and the axial flowing of tube ends is almost synchronous. The results are larger deformation depth with less occurrence of cracking compared with the cases of short pulse width, as shown in Fig. 24, and the good profile of the deformed tube, as shown in Fig. 22.

Therefore, the shorter the pulse width of the middle-coil current, the larger the deformation depth of the tube under equal discharging energy, but the higher occurrence of the cracking and worse tube profile. The longer the pulse width of the middle-coil current, the better the profile of the deformed tube, and the occurrence of cracking is less under the same deformation depth compared with the shorter pulse width. It can be concluded that the short pulse width of the middle-coil current can achieve larger deformation depth of the tube under relatively small discharging energy, while the long pulse width of the middle-coil current can achieve the higher requirement of the tube profile and deforming quality.

5 Conclusion

In this work, the deformation behavior of tube under different pulse width of middle-coil current in two-stage coils system is studied, and the effect of the pulse width of middle-coil current is discussed. Results show that the short pulse width of the middle-coil current can achieve larger deformation depth of the tube under relatively small discharging energy, and the long pulse width of the middle-coil current has good performance in the deformed profile. What is more, the thickness reduction in the case of long pulse width of the middle-coil current is less than the case of short pulse width of the middle-coil current under equal deformation depth of the tube. More investigations and significant results of the two-stage coils system will be further developed through simulations and experiments in the future.

Compliance with ethical standards

References

1. Psyk V, Risch D, Kinsey BL, Tekkaya AE, Kleiner M (2011) Electromagnetic forming-a review. J Mater Process Technol 211(5):787–829

2. Cao QL, Du LM, Li ZH, Lai ZP, Li ZZ, Chen M, Li XX, Xu SF, Chen Q, Han XT, Li L (2019) Investigation of the Lorentz-force-driven sheet metal stamping process for cylindrical cup forming. J Mater Process Technol 271:532–541

3. Qiu L, Yi NX, Abu-Siada A, Tian JP, Fan YW, Deng K, Xiong Q, Jiang JB (2020) Electromagnetic force distribution and forming performance in electromagnetic forming with discretely driven rings. IEEE Access 8:16166–16173. https://doi.org/10.1109/ACCESS.2020.2967096

4. Lai ZP, Cao QL, Han XT, Huang YJ, Deng FX, Chen Q, Li L (2017) Investigation on plastic deformation behavior of sheet work-piece during radial Lorentz force augmented deep drawing process. J Mater Process Technol 245:193–206

5. Huang LT, Zhang J, Zou JH, Zhou YH, Qiu L (2019) Effect of equivalent radius of drive coil on forming depth in electromagnetic sheet free bulging. Int J Appl Electrom 61:377–389

6. Xiong Q, Huang H, Xia LY, Tang HT, Qiu L (2019) A research based on advance dual-coil electromagnetic forming method on flanging of small-size tubes. Int J Adv Manuf Technol 102:4087–4094

7. Kinsey B, Nassiri A (2017) Analytical model and experimental investigation of electromagnetic tube compression with axisymmetric coil and field shaper. CIRP Ann-Manuf Techn 66: 273–276

8. Xiong Q, Tang HT, Wang MX, Huang H, Qiu L, Yu K, Chen Q (2019) Design and implementation of tube bulging by an attractive electromagnetic force. J Mater Process Technol 273:116240

9. Park H, Lee J, Lee Y, Kim JH, Kim D (2019) Electromagnetic expansion joining between tubular and flat sheet component. J Mater Process Technol 273:116246

10. Li Z, Liu SJ, Li JP, Wang M (2018) Effect of coil length and relative position on electromagnetic tube bulging. Int J Adv Manuf Technol 97:379–387

11. Qiu L, Yu YJ, Xiong Q, Deng CZ, Cao QL, Han XT, Li L (2018) Analysis of electromagnetic force and deformation behavior in electromagnetic tube expansion with concave coil based on finite element method. IEEE T Appl Supercon 28(3):0600705

12. Cui XH, Mo JH, Li JJ, Xiao XT (2017) Tube bulging process using multidirectional magnetic pressure. Int J Adv Manuf Technol 90(5–8):2075–2082

13. Qiu L, Li YT, Yu YJ, Xiao Y, Su P, Xiong Q, Jiang JB, Li L (2019) Numerical and experimental investigation in electromagnetic tube expansion with axial compression. Int J Adv Manuf Technol 104: 3045–3051

14. Lai ZP, Cao QL, Zhang B, Han XT, Zhou ZY, Xiong Q, Zhang X, Chen Q, Liang L (2015) Radial Lorentz force augmented deep drawing for large drawing ratio using a novel dual-coil electromagnetic forming system. J Mater Process Technol 222:13–20

15. Zhang X, Cao QL, Han XT, Chen Q, Lai ZP, Xiong Q, Deng FX, Li L (2016) Application of triple-coil system for improving deformation depth of tube in electromagnetic forming. IEEE T Appl Supercon 26(4):3701204

16. Zhang X, Li CX, Wang XG, Zhao Y, Li L (2019) Improvement of deformation behavior of tube in electromagnetic forming with a triple-coil system. Int J Appl Electrom 61(2):263–272

17. Zhang X, Cao QL, Li XX, Yi L, Ma JM, Li XH, Li L (2018) Deformation behavior of tube in electromagnetic forming with an external die. Int J Appl Electrom 57(4):377–388

18. Cao QL, Han XT, Lai ZP, Xiong Q, Zhang X, Chen Q, Xiao HX, Li L (2015) Analysis and reduction of coil temperature rise in electromagnetic forming. J Mater Process Technol 225:185–194

19. Yu HP, Li CF, Deng JH (2009) Sequential coupling simulation for electromagnetic-mechanical tube compression by finite element analysis. J Mater Process Technol 209:707–713

20. Cao QL, Li ZH, Lai ZP, Li ZZ, Han XT, Li L (2019) Analysis of the effect of an electrically conductive die on electromagnetic sheet metal forming process using the finite element-circuit coupled method. Int J Adv Manuf Technol 101:549–563

21. Liu SB, Ruan JJ, Peng Y, Zhang YJ, Zhang YD (2011) Improvement of current filament method and its application in performance analysis of induction coil gun. IEEE T Plasma Sci 39(1):382–389

22. Mamalis AG, Manolakos DE, Kladas AG, Koumoutsos AK (2006) Electromagnetic forming tools and processing conditions: numerical simulation. Mater Mauf Process 21(4):411–423